

# Enhancing the Cyclability of $\text{VS}_4$ Positive Electrode in Carbonate-Based Electrolyte using Fluoroethylene Carbonate Additive

Kazuki Yoshii,<sup>\*[a]</sup> Kazushige Kohno,<sup>[a]</sup> Yuta Maeyoshi,<sup>[a]</sup> Noboru Taguchi,<sup>[a]</sup> Akira Yano,<sup>[a]</sup> Tomonari Takeuchi,<sup>[a]</sup> and Hikari Sakaeb<sup>[a]</sup>

Vanadium polysulfide ( $\text{VS}_4$ ) is a promising material of construction for positive electrodes of next-generation batteries due to its high theoretical capacity and electrical conductivity compared to those of elemental sulfur. In this study, we investigated the charge and discharge behavior of a low-crystalline  $\text{VS}_4$  positive electrode using different electrolytes and under differing charge and discharge conditions. The electrolyte composed purely of cyclic carbonate exhibited higher cycle performance than the one containing linear carbonate. Further-

more, the addition of fluoroethylene carbonate (FEC) to the electrolyte was very effective to improve the cycle performance. The effects of FEC on the  $\text{VS}_4$  positive electrode were investigated using electrochemical techniques, X-ray photoelectron spectroscopy, and electron microscopy, the results whereof indicated that LiF-containing components were formed on the  $\text{VS}_4$  surface, and probably contributed to the improvement of the charge and discharge behavior of the  $\text{VS}_4$  positive electrode.

## Introduction

The development of lithium rechargeable batteries having high energy densities is urgently required to popularize electric vehicles and smaller, more powerful portable electronic devices.<sup>[1]</sup> Transition metal oxides, elemental sulfur, and metal fluorides have been actively investigated as positive electrode materials to realize batteries having high energy densities.<sup>[2]</sup> Elemental sulfur has a high potential for practical use because of its resource advantages and high theoretical capacity.<sup>[3]</sup> However, sulfur has a low electrical conductivity, and lithium polysulfide dissolves into the electrolyte during charge and discharge reactions, making it difficult to simultaneously achieve high energy densities and stable cycle performance.

Transition metal polysulfides are also attracting attention as electrode active materials because of their high theoretical capacity and high electric conductivities compared to elemental sulfur, which facilitate the realization of batteries having high energy densities.<sup>[4]</sup> While various types of transition metal polysulfides have been investigated as electrode active materials,  $\text{VS}_4$  has been recognized as a particularly promising candidate for lithium, aluminum, magnesium, and calcium secondary batteries.<sup>[5]</sup> Rout et al. reported a composite of  $\text{VS}_4$  and reduced graphene oxide (rGO) prepared by hydrothermal

reaction using sodium orthovanadate and thioacetamide that exhibited good cycle performance when used to fabricate the negative electrodes of lithium secondary batteries.<sup>[5a]</sup> Britto et al. investigated the unique lithiation and de-lithiation mechanisms of  $\text{VS}_4$  by conducting nuclear magnetic resonance (NMR) and X-ray analyses.<sup>[5b]</sup> Recently, it was suggested that  $\text{VS}_4$  supported on rGOs and nitrogen-doped carbon nanotubes acts as a polysulfide mediator by offering sufficient polysulfide-anchoring and catalytic sites, facilitating the construction of high-loading lithium-sulfur (Li-S) batteries.<sup>[6]</sup>

Our research group has been exploring the potential of  $\text{VS}_4$  as a positive electrode material for Li-S batteries having energy densities exceeding  $500 \text{ Wh kg}^{-1}$ .<sup>[7]</sup>  $\text{VS}_4$  prepared by thermal treatment in vacuum has exhibited high discharge capacities (exceeding  $900 \text{ mAh g}^{-1}$ ) in carbonate-based electrolytes.<sup>[7a]</sup> We also found that the low crystallinity of  $\text{VS}_4$  increases the Coulombic efficiency in the initial cycle, which in turn improves the cycle stability.<sup>[7b]</sup> Furthermore, we have established that the capacity retention ratio can be improved by doping elemental phosphorus into low-crystalline  $\text{VS}_4$  and by utilizing a localized high-concentration carbonate-based electrolyte containing lithium bis(fluorosulfonyl)imide.<sup>[7c,d]</sup> However, the cycling ability of  $\text{VS}_4$  electrodes remains insufficient for practical use, and needs to be improved further. One of the strategies to improve the cycle ability of the batteries is the use of additives in the electrolyte, and various additives have been investigated for sulfur-based positive electrode. Among them, fluoroethylene carbonate (FEC), which is well known to improve the cycle ability of negative electrode materials by forming LiF-rich solid electrolyte interphase,<sup>[8]</sup> has been reported as an effective additive to the Li-S batteries.<sup>[9]</sup>

In this study, we investigated the electrolyte composition and charge and discharge conditions to improve the cycle performance of low-crystalline  $\text{VS}_4$ . The cycle performance

[a] Dr. K. Yoshii, Dr. K. Kohno, Dr. Y. Maeyoshi, Dr. N. Taguchi, Dr. A. Yano, Dr. T. Takeuchi, Dr. H. Sakaeb  
Research Institute of Electrochemical Energy (RIEKEN)  
Department of Energy and Environment  
National Institute of Advanced Industrial Science and Technology (AIST)  
1-8-31 Midorigaoka, Ikeda, Osaka 563-8577, Japan  
E-mail: k.yoshii@aist.go.jp

 Supporting information for this article is available on the WWW under  
<https://doi.org/10.1002/batt.202200016>

 An invited contribution to a Special Collection dedicated to Lithium-Sulfur Batteries.

varied with the type of carbonate. FEC was also investigated as an additive for the electrolyte, and it was verified that the addition of FEC improved the cycle performance. We believe that this paper provides a strategy for improving the charge and discharge performances of the batteries using metal polysulfide as a positive electrode.

## Results and Discussion

$\text{VS}_4$  used for electrochemical measurements was confirmed to exhibit lower crystallinity than that before the mechanical milling process by powder X-ray diffraction, and was found to contain  $\text{V}_2\text{O}_3$  derived from the initial  $\text{V}_2\text{S}_3$ , as reported previously.<sup>[7b]</sup> A reaction mechanism was propounded in which  $\text{VS}_4$  is lithiated to  $\text{Li}_{3+x}\text{VS}_4$  upon discharge, and the conversion

reaction proceeds in the voltage range lower than 1 V.<sup>[5b]</sup> Therefore, in the present study, the charge and discharge tests were conducted in the voltage range of 1.5–2.6 V, at which the conversion reaction does not proceed. Figure 1(a–d) shows the charge and discharge profiles of the  $\text{VS}_4$  positive electrode cell using four types of electrolytes: 1.0 M (=mol dm<sup>-3</sup>) lithium bis(trifluoromethanesulfonyl)amide (LiTFSAs)/ethylene carbonate (EC):dimethyl carbonate (DMC)(1:1), 1.0 M LiTFSAs/EC:propylene carbonate (PC)(1:1), 1.0 M LiPF<sub>6</sub>/EC:DMC(1:1), and 1.0 M LiPF<sub>6</sub>/EC:PC(1:1). Irrespective of the type of lithium salt and organic electrolyte used, all the cells exhibited a discharge capacity of approximately 800 mAh g<sup>-1</sup> in the initial cycle, allowing continuous charge and discharge cycling. Figure 1(e and f) shows the changes in the discharge capacity and Coulombic efficiency of the cells. In the case of both the lithium salts, the cycle performance in the EC:PC(1:1)-based electrolyte

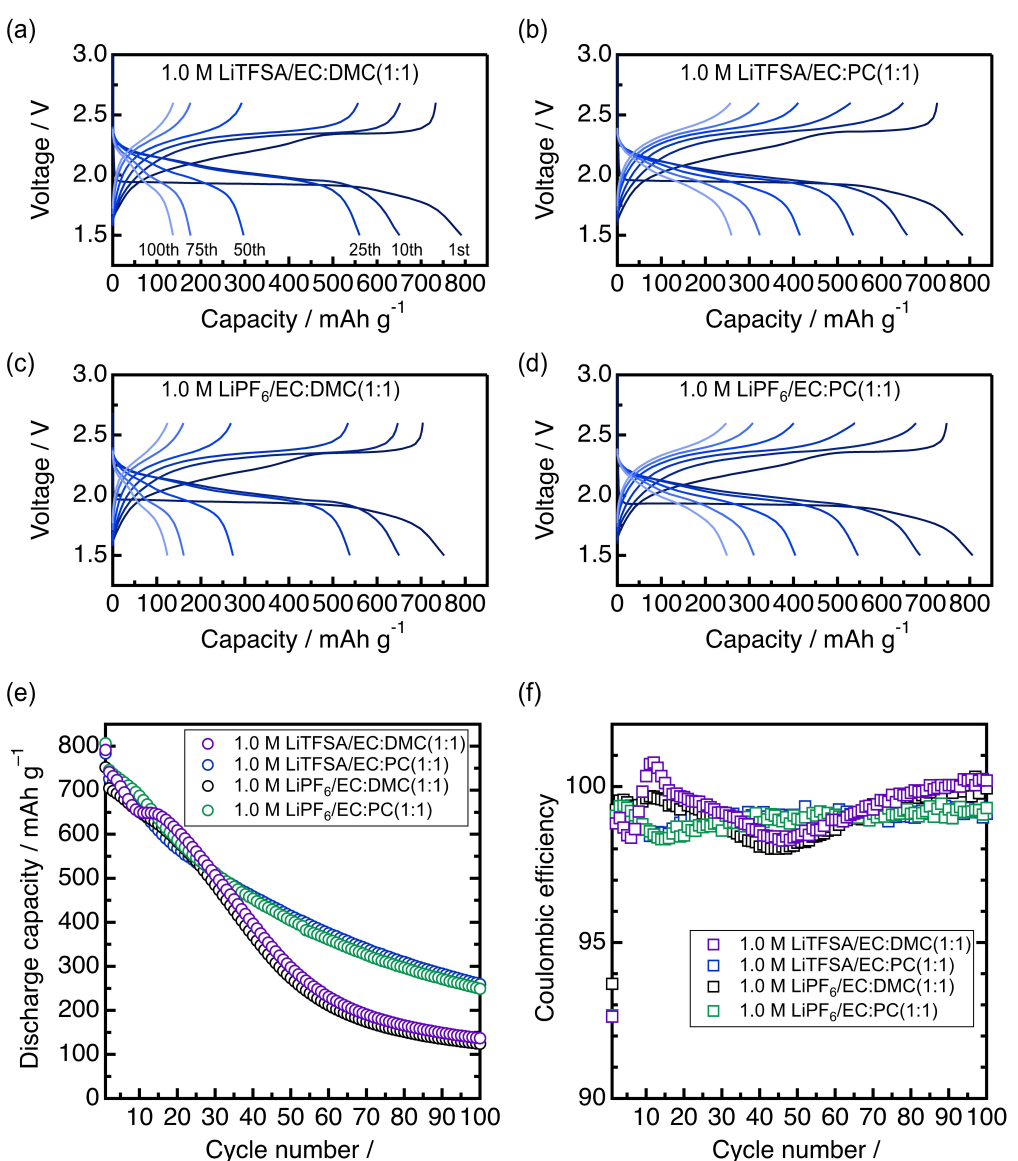


**Figure 1.** Charge and discharge profiles of  $\text{VS}_4$  positive electrode in a) 1.0 M LiTFSAs/EC:DMC(1:1), b) 1.0 M LiTFSAs/EC:PC(1:1), c) 1.0 M LiPF<sub>6</sub>/EC:DMC(1:1), and d) 1.0 M LiPF<sub>6</sub>/EC:PC(1:1). Plots of e) discharge capacity and f) Coulombic efficiency against the cycle number for the cell using each electrolyte. The voltage range for charge and discharge cycling was 1.5–2.6 V.

was superior to that in the EC:DMC(1:1)-based electrolyte. The Coulombic efficiency also remained stable at approximately 99% in the EC:PC(1:1)-based electrolyte. This may have resulted from the difference in the reactivity of  $\text{VS}_4$  with PC and DMC. Our research group has previously reported that sulfur-containing carbonate oligomers are formed in 1.0 M  $\text{LiPF}_6$ /EC:DMC(1:1) following charge and discharge testing when using  $\text{Li}_x\text{FeS}_5$ , which is a transition metal sulfide, as the positive electrode.<sup>[10]</sup> Although the sulfur components were not leached from the metal polysulfide into the electrolyte as a polysulfide, the formation of the oligomers containing sulfur and carbonates is considered to be one of the processes responsible for capacity decay. Furthermore, computational chemistry investigations have recently revealed that PC is less reactive toward  $\text{VS}_4$  than DMC.<sup>[11]</sup> We infer therefrom that the elution of sulfur from the electrode was lower in the EC:PC(1:1)-based electrolyte, which improved the cycle performance. An electrolyte containing solely cyclic carbonate has higher viscosity and lower ionic conductivity compared to one that contains linear carbonate. However, it is considered to be useful because of its lower reactivity with the active materials that comprise the electrodes. The results shown above evinced no significant difference between the cycle performance of LiTFSA and  $\text{LiPF}_6$ . However, the presence of a small amount of moisture in the electrolyte containing  $\text{LiPF}_6$  can cause the generation of HF,<sup>[12]</sup> which may lead to the elution of transition metals from the active materials and the formation of a high-resistance film on the lithium metal negative electrode. To avoid this risk, 1.0 M LiTFSA/EC:PC(1:1) was used in the subsequent experiments.

Various compounds have been investigated as additives to the electrolyte in lithium batteries. Among them, FEC is particularly effective in improving the cycle performance of graphite, lithium metal, and silicon negative electrodes, and transition metal oxide positive electrodes.<sup>[8b,9a,c,13]</sup> In our previous study, we have reported that the addition of FEC to 1.0 M LiTFSA/EC:PC(1:1) improves the cycle performance of lithium metal anodes.<sup>[8c,d]</sup> Therefore, the effect of FEC addition to the electrolyte on the  $\text{VS}_4$  positive electrode was investigated. Figure 2(a and b) shows the changes in the discharge capacity and Coulombic efficiency of the  $\text{VS}_4$  positive electrode using 1.0 M LiTFSA/EC:PC(1:1) upon the addition of 5 wt% FEC. Although the discharge capacity for the initial cycle was similar to that in the electrolyte without FEC, the decay of the discharge capacity as the number of cycles increased was suppressed. The discharge capacity retention ratio against the 2nd cycle at the 100th cycle was 66.3% in the electrolyte containing FEC, in contrast to 35.7% in the electrolyte without FEC (calculated from the result depicted in Figure 1e). Because this experiment was conducted in a half-cell, i.e., the utilization ratio of the lithium metal negative electrode was sufficiently low, it is inferred that FEC is effective at increasing the cycle stability of a  $\text{VS}_4$  positive electrode, which will be reexamined later. We have also verified the discharge rate capability of  $\text{VS}_4$  positive electrode. Discharge profiles with different current densities after three cycles of discharge and charge were shown in Figure S1 using the electrolytes with and without FEC. It has been reported that  $\text{VS}_4$  exhibits better rate

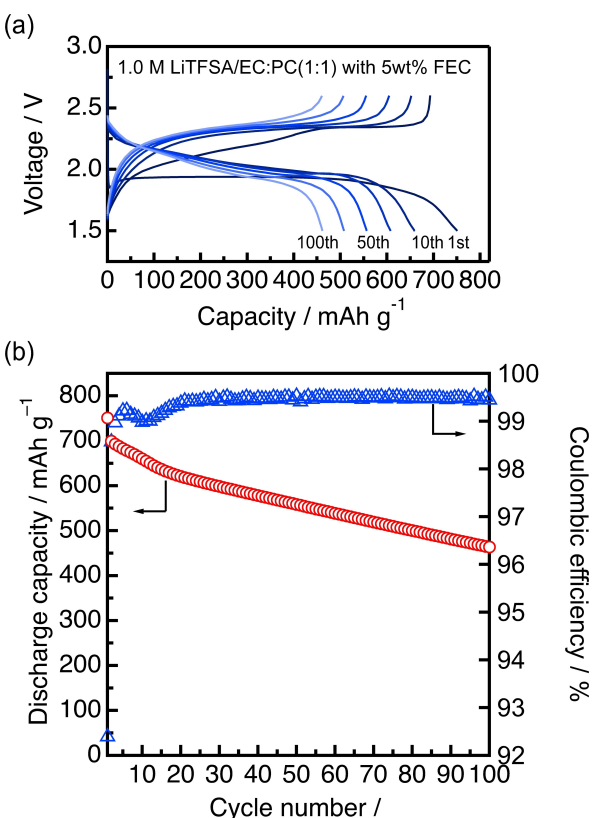


Figure 2. a) Charge and discharge profiles of the  $\text{VS}_4$  positive electrode in 1.0 M LiTFSA/EC:PC(1:1) containing 5 wt% of FEC. b) Plot of discharge capacity and Coulombic efficiency against the cycle number. The voltage range for the charge and discharge cycling was 1.5–2.6 V.

capability,<sup>[5a]</sup> and in our experiments, satisfactory capacity retention was observed up to a current density of 1400  $\text{mA g}^{-1}$  whether FEC was added or not into the electrolyte. When discharged at a very high current density of 2800  $\text{mA g}^{-1}$ , the discharge capacity of 577.4  $\text{mAh g}^{-1}$  was observed in the electrolyte with FEC in contrast to that of 407.3  $\text{mAh g}^{-1}$  in the electrolyte without FEC (Table S1), suggesting that the charge transfer resistance of  $\text{VS}_4$  becomes smaller in the electrolyte with FEC. Therefore, we measured the electrochemical impedance spectroscopy. Figure S2 shows the Nyquist plots obtained after 12 hours of cell assembly and after 1 and 5 charge and discharge cycles. In the plot obtained after 12 hours of cell assembly, lower charge transfer resistance was observed in the electrolyte with FEC, indicating a possibility of the reaction of FEC with  $\text{VS}_4$ . After charge and discharge cycles, the absolute value of resistance was smaller, which is probably due to the increase in surface area of the electrode materials caused by the volume change associated with the charge and discharge reaction. After both 1st and 5th cycles, the charge transfer resistance was clearly smaller when the electrolyte with FEC was used, suggesting that favorable interface capable of discharging at a large current density was formed on the electrode.

During the charge and discharge tests in the voltage range of 1.5–2.6 V,  $\text{VS}_4$  was lithiated to  $\text{Li}_{3+x}\text{VS}_4$ , resulting in a significant structural change of the active material, which was

considered to be one of the processes responsible for the decay of the discharge capacity. Therefore, the charge and discharge behavior in the low depth of discharge region was investigated. Following two cycles of aging in the voltage range of 1.5–2.6 V, charge and discharge cycling was performed in the voltage range of 1.9–2.6 V. The charge and discharge curves of the  $\text{VS}_4$  positive electrode using 1.0 M LiTFS/EC:PC(1:1) with and without FEC as the electrolyte and the change of the discharge capacity and Coulombic efficiency are plotted against the cycle number in Figure 3. In the case of the cell using 1.0 M LiTFS/EC:PC(1:1), the discharge capacity decreased following the first few cycles, whereafter charging and discharging proceeded with a Coulombic efficiency exceeding 99%, and a discharge capacity of 250 mAh g<sup>-1</sup> was retained following 100 cycles. In contrast, for the cell using 1.0 M LiTFS/EC:PC(1:1) with 5 wt% of FEC as the electrolyte, the charging and discharging proceeded with a Coulombic efficiency exceeding 99.5%. A discharge capacity of 465 mAh g<sup>-1</sup> was retained following the 100th cycle, and the capacity retention ratio against the initial cycle was 91.0%. When charging and discharging was conducted in the voltage range of 1.9–2.6 V, the discharge capacity decreased initially but increased thereafter, irrespective of the presence or absence of FEC. At present, the reason for this behavior has not been analyzed and remains a speculation; however, it is hypothesized to occur due to structural changes of the active material. As described above, charge and discharge tests were conducted in two different voltage ranges, and the results proved the effectiveness of FEC in both voltage ranges at improving the capacity retention of  $\text{VS}_4$  positive electrodes. The results of this study were good compared to the previously reported cycle performance of  $\text{VS}_4$  as a positive electrode material (Table S2).

To further investigate the effect of FEC on  $\text{VS}_4$  positive electrodes, charge and discharge tests were conducted using a three-electrode cell.  $\text{VS}_4$ , lithium foil, and lithium wire were used as the working electrode (WE), counter electrode (CE), and reference electrode (RE), respectively. The tests were controlled

at the potential of WE-RE. Figure 4(a) shows the voltage and potential profiles of WE-RE, WE-CE, and CE-RE at the 10th and 80th cycles (The voltage and potential profiles from the initial cycle to the 100th cycle are shown in Figure S3). Figure 4(b) plots the change of discharge capacity against cycle number, as read from the profile of WE-RE, which was consistent with that obtained from the two-electrode cell. The difference in the overpotential between the electrolytes with and without FEC observed from the potential profiles of CE-RE during discharge suggested that FEC facilitated the reaction at the lithium metal negative electrode. In our previous work, we reported the cycle performance of Li metal anode in 1.0 M LiTFS/EC:PC (1:1), proving that FEC improves the cycle stability even at high lithium utilization.<sup>[8c,d]</sup> However, the overpotential at the 80th cycle was approximately 30 mV even in the absence of FEC, from which we infer that the increase in overpotential was insufficient to contribute significantly to the decay in the discharge capacity of the cell. This indicates that FEC is effective in improving the reversibility of the  $\text{VS}_4$  cathode reaction. The cyclic voltammograms of WE-RE recorded using the three-electrode cell are plotted in Figure 4(c). The onset potentials of the reduction current in the 1st cycle were similar irrespective of the presence or absence of FEC. However, following the second cycle, the reduction current was observed from a higher potential in the electrolyte containing FEC, suggesting that FEC reacts with  $\text{VS}_4$  at approximately 2.1 V vs. Li/Li(I). The lowest unoccupied molecular orbital (LUMO) of FEC is lower than those of EC and PC, leading to its decomposition in the higher potential region.<sup>[8b]</sup> Although FEC reacts at approximately 2.1 V vs. Li/Li(I) on graphite anode and 0.6 V vs. Li/Li(I) on  $\text{MoS}_2$ , it is considered to react with  $\text{VS}_4$  in a higher potential region.<sup>[9c,13a]</sup> To confirm the aforementioned observations, inferences, and hypotheses, we used a two-compartment cell. The cell contained a lithium-ion conducting glass-ceramic separator between the positive and negative electrodes. Therefore, its electrochemical behavior could be evaluated by separating the effects of the electrolyte on the positive and negative electrodes.<sup>[14]</sup> Figure 5 plots the discharge capacity of the  $\text{VS}_4$

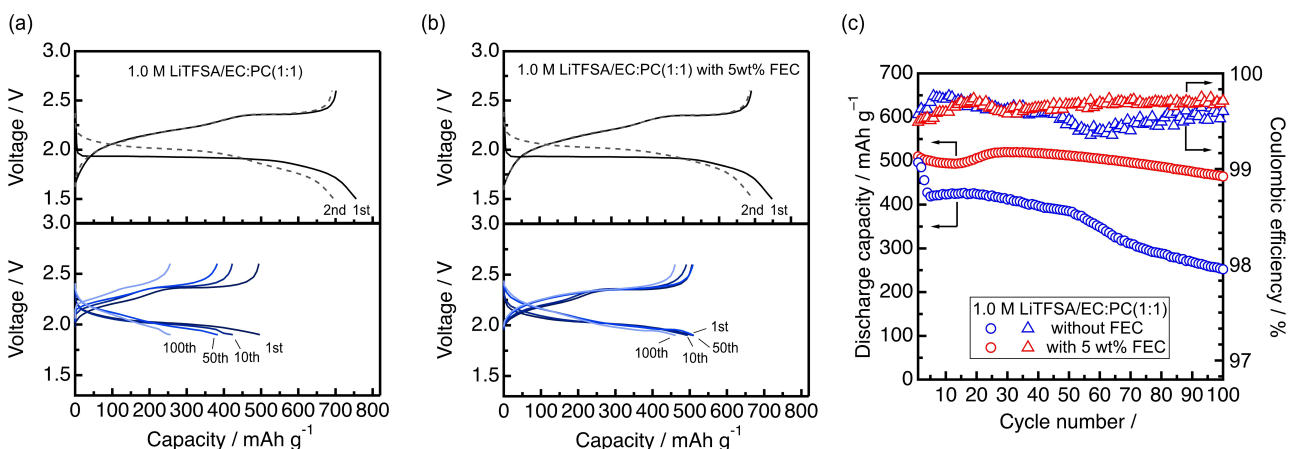


**Figure 3.** Charge and discharge profiles of  $\text{VS}_4$  positive electrodes in a) 1.0 M LiTFS/EC:PC(1:1) and b) 1.0 M LiTFS/EC:PC(1:1) with 5 wt% of FEC. The upper plot shows the first two cycles, operated in the voltage range of 1.5–2.6 V. The lower graph shows the profiles obtained in the voltage range of 1.9–2.6 V. c) Plots of discharge capacity and Coulombic efficiency against the cycle number.

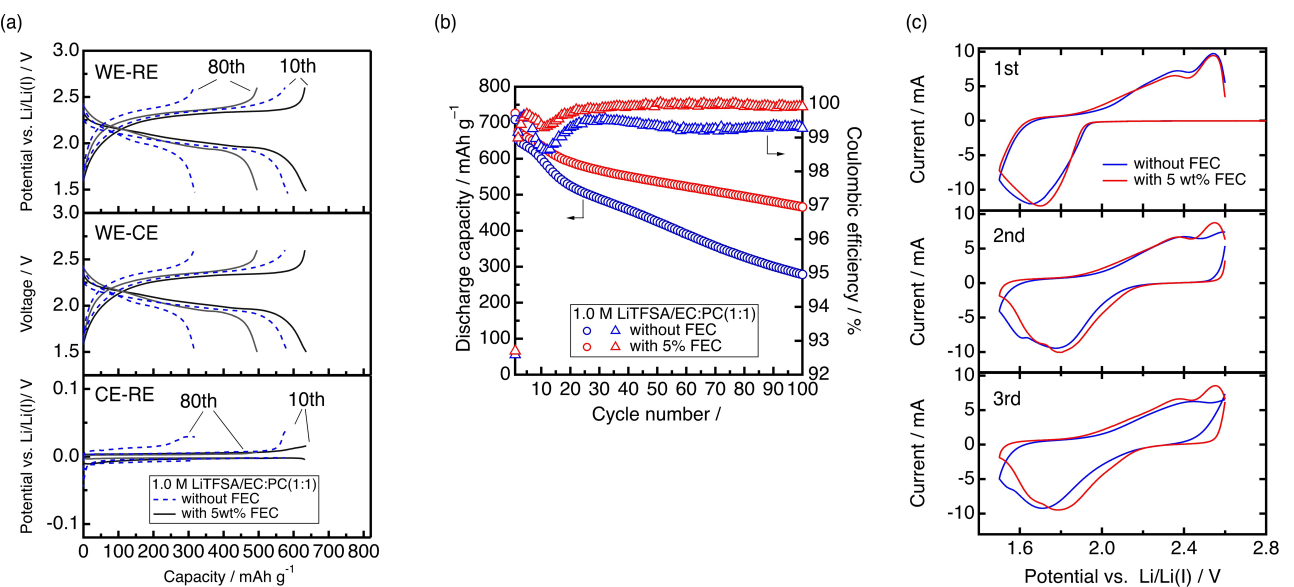


**Figure 4.** a) Potential and voltage profiles of three-electrode cell using 1.0 M LiTFSa/EC:PC(1:1) with and without 5 wt% of FEC. top) WE-RE, middle) WE-CE, bottom) CE-RE. b) Plots of discharge capacity and Coulombic efficiency against the cycle number. The voltage range for the charge and discharge cycling was 1.5–2.6 V. c) Cyclic voltammograms of the VS<sub>4</sub> electrode recorded using the three-electrode cell.

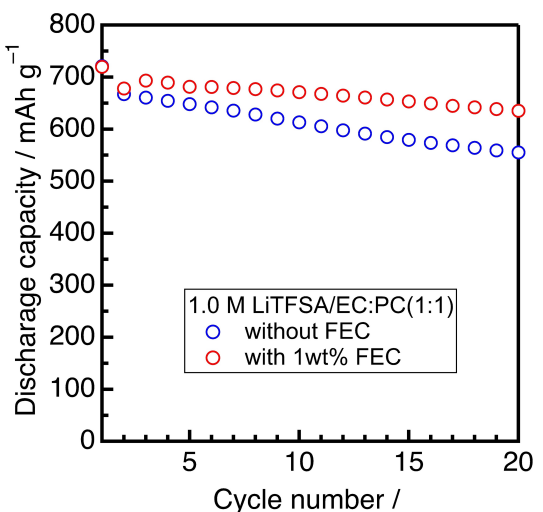


**Figure 5.** Plots of discharge capacity against cycle number for the two-compartment cell using electrolytes with and without FEC in the positive electrode compartment only. The voltage range for charge and discharge cycling was 1.5–2.6 V.

composite electrode against the cycle number in the two-compartment cell using 1 wt% FEC as the additive for the electrolyte of the positive electrode compartment and in the absence of the additive. A clear difference in the discharge capacity became evident following 20 cycles, which confirmed that FEC is effective at improving the cycle stability of VS<sub>4</sub> positive electrodes.

To examine how FEC improves the cycle performance of VS<sub>4</sub>, the electrode disassembled from the cell after 30 cycles was analyzed using scanning electron microscopy (SEM), X-ray photoelectron spectroscopy (XPS), and scanning transmission electron microscope (STEM). Figure S4 shows the SEM images

of the electrodes following charge and discharge cycling using electrolytes with and without FEC; there was no significant difference in the appearance of the two, although there was mild cracking in the electrode used in the electrolyte without FEC, which was probably caused by the expansion of the active material during the discharge reaction. Figure 6 shows the XPS spectra of the VS<sub>4</sub> electrode following charge and discharge cycling while immersed in electrolytes with and without FEC, accompanied by the spectrum of the pristine sample. In the C1s spectra, peaks attributed to carbonate and CF<sub>3</sub> groups derived from the electrolyte and LiTFSa present in the electrolyte without FEC appeared with stronger intensities than those in the electrolyte containing FEC, implying that the deposition of electrolyte decomposition products on the positive electrode occurs when the electrolyte lacks FEC. In the F1s region, peaks corresponding to LiF and the SO<sub>2</sub>-CF<sub>3</sub> group derived from the TFSa anion were observed in the spectrum of the electrode immersed in the electrolyte without FEC. In contrast, for the electrode immersed in the electrolyte containing FEC, a broad peak appeared at approximately 685–690 eV. At present it is difficult to accurately attribute this peak. The polymer component containing the CF<sub>2</sub> group generates peaks at approximately 687 eV in the F1s region and at approximately 290 eV in the C1s region.<sup>[15]</sup> The present XPS spectra suggested the formation of compounds containing CF<sub>2</sub> groups, although no evidence for this has been obtained from the other measurements, and it remains a matter of speculation. Figure S5 shows the XPS spectra of Li1s, N1s, O1s, S2p, and V2p.<sup>[7c]</sup> In the Li1s spectra, the peak attributed to LiF was observed. In the N1s and S2p regions, intense TFSa anion-derived peaks were identified in the spectra of the electrode immersed in the electrolyte without FEC, which agreed closely with the F1s spectral analysis. The peaks appearing at the binding energies corresponding to C=O, C—O, and sulfates were observed in the

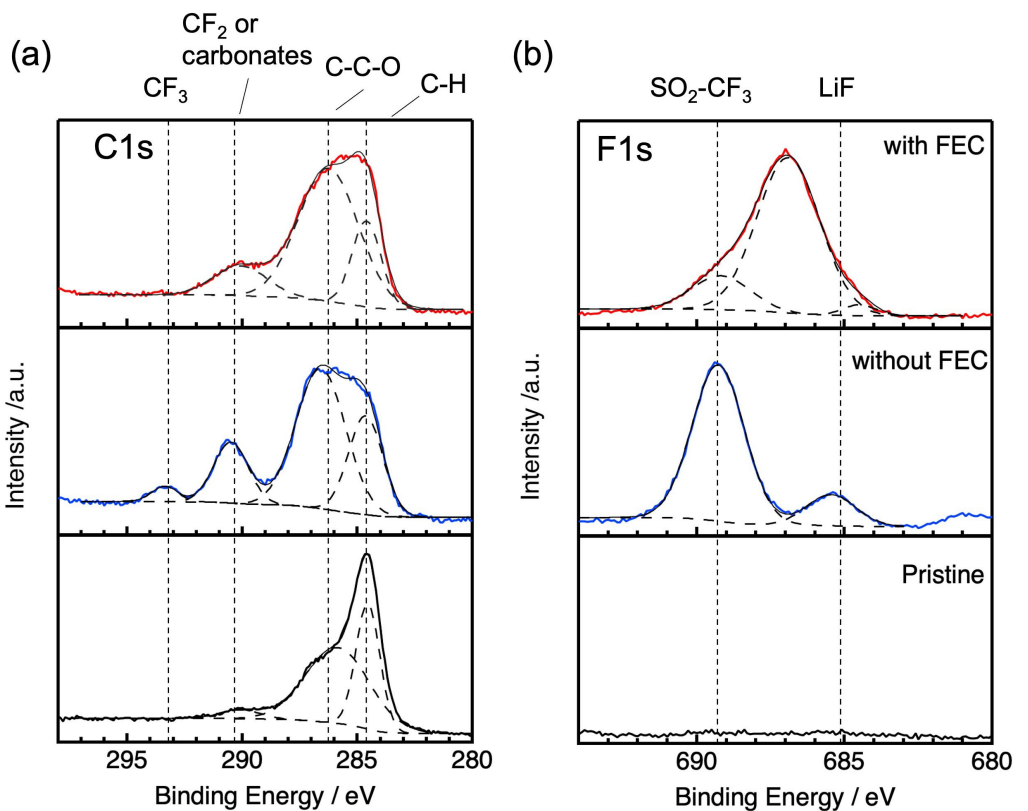
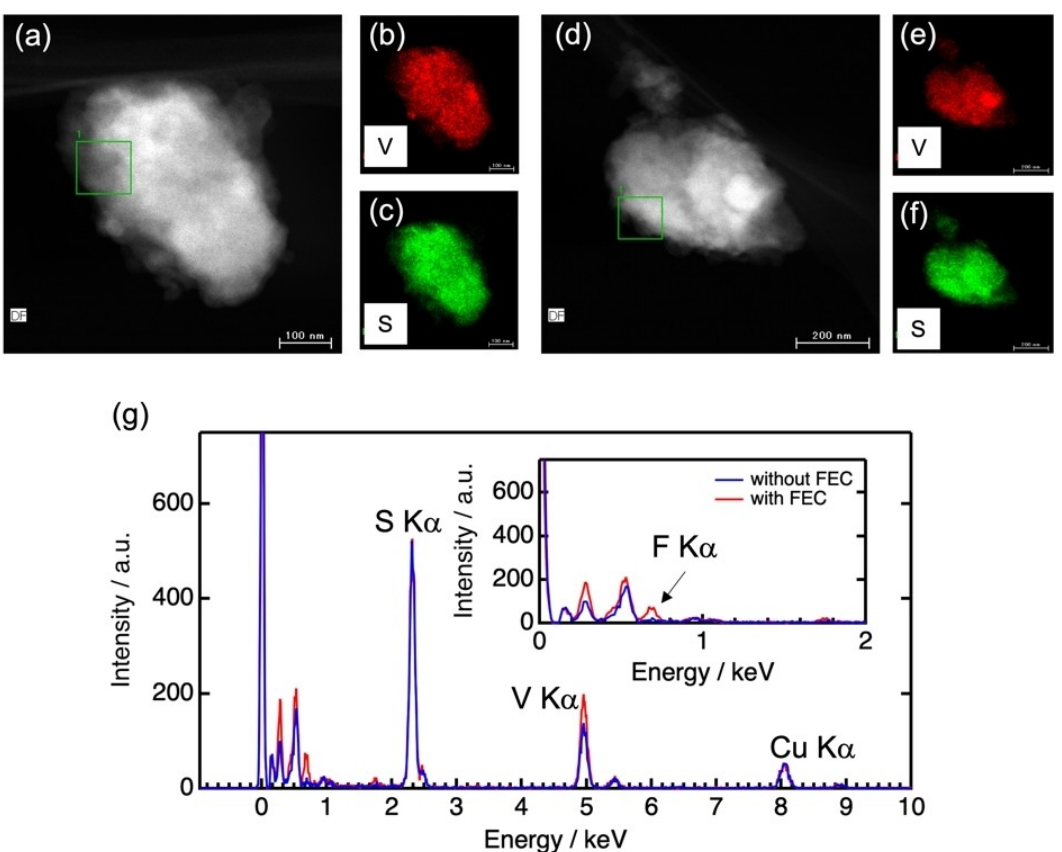


**Figure 6.** a) C1s and b) F1s XPS spectra of the  $\text{VS}_4$  electrodes before and after 30 charge and discharge cycles using 1.0 M LiTFSa/EC:PC(1:1) with and without 5 wt% of FEC as the electrolyte.

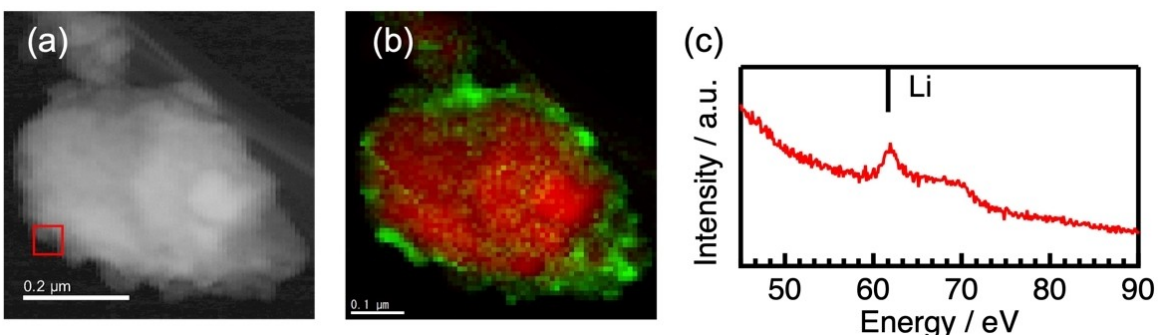
O1s region. In the V2p spectrum, the peak corresponding to  $\text{V}^{4+}$  appeared before charge and discharge cycling; however, its intensity decreased following cycling, suggesting that the compounds formed by the decomposition of the electrolyte are deposited on the active material. From the aforementioned results, in the differences between the peak intensities derived from the decomposition products of TFSa anions in the electrolyte with and without FEC become evident, suggesting that the decomposition of the electrolyte may be suppressed by the addition of FEC.

Figure 7 shows the STEM images and energy-dispersive X-ray spectroscopy (EDS) elemental maps of a  $\text{VS}_4$  particle following 30 cycles of charging and discharging while immersed in electrolytes with and without FEC. Figure 7(g) shows the EDS spectra obtained from the part of the green squares shown in Figure 7(a and d). In the EDS spectra, peaks attributed to  $\text{S K}_{\alpha}$  and  $\text{V K}_{\alpha}$  derived from  $\text{VS}_4$  and  $\text{Cu K}_{\alpha}$  from the grid were identified. Focusing on the low-energy region expanded in the inset of Figure 7(g), the peak of  $\text{F K}_{\alpha}$  at approximately 0.67 eV showed a clear difference depending on the presence or absence of FEC in the electrolyte. We hypothesized that F-containing compounds were formed on the surface of the active material when the electrolyte containing FEC was used. Figure 8(a and b) shows the annular dark-field (ADF) image of  $\text{VS}_4$  and the overlapped concentration mapping image of the Li K-edge following 30 cycles of charging and discharging while immersed in the electrolyte

containing FEC, which indicates the presence of Li-containing species on the surface of the active material particles. Figure 8(c) depicts the EELS spectrum of the Li K-edge region obtained from the red square in Figure 8(c), which shows a characteristic peak of LiF.<sup>[16]</sup> In contrast, no Li-containing compound was observed in  $\text{VS}_4$  following charge and discharge cycling while immersed in the electrolyte without FEC (Figure S6a and b). The electron energy-loss spectroscopy (EELS) spectra in the Li K-edge region showed no peaks characteristic of LiF (Figure S6c). Since all the samples observed by STEM were observed following charging, it is possible that a large amount of  $\text{Li}_x\text{VS}_4$  did not return to  $\text{VS}_4$  upon charging while immersed in the electrolyte without FEC. These results suggest a possibility that the LiF-containing components on the active material surface contribute to the improvement of the cycle characteristics when the electrolyte contains FEC. It has been reported that the surface coating of  $\text{Li}_8\text{FeS}_5$  by  $\text{TiO}_x$  improves cycle performance due to the suppression of electrolyte decomposition.<sup>[17]</sup> The computational chemistry approach also shows that the electrolyte decomposition proceeds on the  $\text{VS}_4$  positive electrode even when the electrolyte contains a cyclic carbonate.<sup>[11]</sup> In the electrolyte containing FEC, the component including LiF on the electrode surface generated by the decomposition of FEC may inhibit the decomposition of the electrolyte and the leaching of V from  $\text{VS}_4$ , which we plan to investigate further in subsequent studies.



**Figure 7.** ADF images of a VS<sub>4</sub> particle extracted from the electrode following 30 cycles of charging and discharging cycle using a) 1.0 M LiTFSAs/EC:PC(1:1) and b) 1.0 M LiTFSAs/EC:PC(1:1) containing FEC as the electrolytes. Overlapped concentration-mapping images of b, d) V K<sub>α</sub> and c, f) S K<sub>α</sub>. g) EDS spectrum from the spot shown in (a) and (d).



**Figure 8.** STEM images and EELS characterization. a) ADF images of the VS<sub>4</sub> particle following 30 cycles of charge and discharge cycle using 1.0 M LiTFSAs/EC:PC(1:1) containing 5 wt% FEC as the electrolyte. b) Overlapped concentration-mapping image of Li K-edge. c) Li K-edge spectrum of the region indicated by the red square in (a).

## Conclusion

This study investigated the charge and discharge behavior of low-crystalline VS<sub>4</sub> using different electrolytes and charge and discharge conditions. The EC- and PC-based electrolyte, which is formed only by cyclic carbonates, exhibited higher cycle performance than the EC- and DMC-based electrolyte, which contains linear carbonate. The cycle performances were further improved when FEC was used as an additive for the electrolyte, with a discharge capacity retention ratio of 66.3% and 91%

following 100 charge and discharge cycles performed in the voltage range of 1.5–2.6 V and 1.9–2.6 V, respectively. Analyses performed using three-electrode and two-compartment cells proved that FEC is effective at improving the cycle stability of VS<sub>4</sub> positive electrodes. The results of XPS and STEM-EELS revealed that F-containing compounds were formed on the surface of VS<sub>4</sub>, and suggested that one of the main components thereof was LiF. How exactly these components function to prevent the capacity degradation of VS<sub>4</sub> is a subject for future study. The analysis of the electrolyte following charge and

discharge cycling is essential because cycling may inhibit the decomposition of the electrolyte on the  $\text{VS}_4$  surface and the leaching of vanadium from the positive electrode. However, the findings of the present study are useful for the construction of next-generation batteries using  $\text{VS}_4$  positive electrodes, and further research on improving their characteristics is expected.

## Experimental Section

### Sample preparation

Low-crystalline  $\text{VS}_4$  was prepared by the mechanical milling of crystalline  $\text{VS}_4$  followed by the execution of a previously reported method.<sup>[7b]</sup> Initially,  $\text{V}_2\text{S}_3$  powder (99%, Kojundo Kagaku) and sulfur (99.9% FUJIFILM Wako Pure Chemical) were mixed at a molar ratio of 1:6 and sealed inside an evacuated glass tube, which was followed by heating at 400°C for 12 h. The resulting material was ground using a mortar, resealed inside an evacuated glass tube, and heated under the aforementioned conditions. Thereafter, it was passively cooled to room temperature, and the excess sulfur was removed by heating at 200°C in vacuum. Subsequently, the crystalline  $\text{VS}_4$  was mechanically milled at 270 rpm for 40 h in an Ar atmosphere using a planetary ball mill (Pulverisette 7, Fritsch) to obtain low-crystalline  $\text{VS}_4$ .

### Electrochemical measurements

The electrode preparation and electrochemical cell assembly were conducted in an Ar-filled glove box (Miwa MFG Co., Ltd., Japan, dew point < 85°C,  $\text{O}_2$  < 1 ppm). The working electrode was prepared by the process described below. The low-crystalline  $\text{VS}_4$ , Ketjen black (EC300 J, Lion Specialty Chemicals Co., Ltd., Japan), and a natural polymer-based binder were mixed at a weight ratio of 85:10:5 in a mortar using dimethyl sulfoxide (Kishida Chemical Co., Ltd, Japan). The as-obtained slurry was coated on carbon-coated Al foil (20  $\mu\text{m}$  thickness) and dried at 80°C in vacuum. The resulting sheet was pressed and punched into disks of 15 mm diameter to be used as electrodes. The mass loading of low-crystalline  $\text{VS}_4$  was approximately 1.7  $\text{mg cm}^{-2}$ .

1.0 M LiPF<sub>6</sub>/EC:DMC (1:1 vol%), 1.0 M LiPF<sub>6</sub>/EC:PC (1:1 vol%), 1.0 M LiTFSAs/EC:DMC (1:1 vol%), 1.0 M LiTFSAs/EC:PC (1:1 vol%) were purchased from Mitsubishi Chemical Co., Ltd., Japan. DMC and FEC were purchased from Kishida Chemical Co., Ltd., Japan. A flat-type cell (SB2A, EC Frontier Co., Ltd., Japan) was assembled using Li metal (600  $\mu\text{m}$  thickness, Honjo Metal Co., Ltd., Japan) as the counter electrode, polypropylene-based separator, and glass fiber filter (GF-A, Whatman Plc., UK) in an Ar-filled glove box. A three-electrode cell (Toyo System Co., Ltd., Japan) was assembled using a lithium foil cut into a strip as the reference electrode, while the counter electrode and separator were identical to those used in the flat-type cell. The two-compartment cell (EC Frontier Co., Ltd., Japan) was assembled using Li metal as the counter electrode and polypropylene separators and lithium-ion conducting glass-ceramics (Ohara Inc., Japan, LICGC™, thickness: 150  $\mu\text{m}$ ) in an Ar-filled glove box.<sup>[14]</sup> The charge and discharge tests were conducted using a battery-testing system (TOSCAT-3100, Toyo System Co., Ltd., Japan) and potentiostat/galvanostat with a frequency response analyzer (Hokuto Denko Co., Japan, HZ-Pro S12). The current density was set at 238  $\text{mA g}^{-1}$  for the charge and discharge tests. Coulombic efficiency was calculated by dividing charge capacity into discharge capacity. Electrochemical AC impedance measurements were conducted at an amplitude of  $\pm 10 \text{ mV}$  within the frequency range of 0.1 to 100 kHz. Following the charge and

discharge tests, the cells were disassembled in an Ar-filled glove box. The electrodes were washed with DMC and dried for subsequent analysis.

### Analyses

The morphology of the electrode was observed using scanning electron microscopy (SEM, JSM-6510LA, JEOL Ltd., Japan). X-ray photoelectron spectroscopy (XPS, JPS-9010MX, JEOL Ltd., Japan) was performed using Mg  $K_{\alpha}$  radiation. Fitting and deconvolution of XPS peaks were conducted by COMPRO12. Electron energy-loss spectroscopy (EELS) was performed using a scanning transmission electron microscope (STEM) (FEI Co., USA, Titan<sup>3</sup> G2 60–300) equipped with an EELS (Gatan, Inc., USA, GIF-Quantum) operating at an accelerating voltage of 300 kV. The sample powder for TEM analysis was obtained from the electrode and directly dispersed on a holey carbon film supported on a Cu mesh for TEM analysis in an Ar environment. The samples were transferred to the electron microscope without exposure to the ambient atmosphere using the transfer holder.

### Acknowledgements

This work was supported by the New Energy and Industrial Technology Development Organization (NEDO) under the "Research and Development Initiative for Scientific Innovation of New Generation Batteries 2 (RISING2) (JPNP16001)".

### Conflict of Interest

The authors declare no conflict of interest.

### Data Availability Statement

The data that support the findings of this study are available from the corresponding author upon reasonable request.

**Keywords:** additive · electrolyte · FEC · lithium-sulfur battery ·  $\text{VS}_4$

- [1] a) J. W. Choi, D. Aurbach, *Nat. Rev. Mater.* **2016**, *1*, 16013; b) R. Schmuch, R. Wagner, G. Hörpel, T. Placke, M. Winter, *Nat. Energy* **2018**, *3*, 267–278; c) Y. Yang, E. G. Okonkwo, G. Huang, S. Xu, W. Sun, Y. He, *Energy Storage Mater.* **2021**, *36*, 186–212.
- [2] a) F. Wu, G. Yushin, *Energy Environ. Sci.* **2017**, *10*, 435–459; b) L. Wang, Z. Wu, J. Zou, P. Gao, X. Niu, H. Li, L. Chen, *Joule* **2019**, *3*, 2086–2102; c) J.-M. Kim, X. Zhang, J.-G. Zhang, A. Manthiram, Y. S. Meng, W. Xu, *Mater. Today* **2021**, *46*, 155–182.
- [3] a) X. Chen, T. Hou, K. A. Persson, Q. Zhang, *Mater. Today* **2019**, *22*, 142–158; b) X. Yang, J. Luo, X. Sun, *Chem. Soc. Rev.* **2020**, *49*, 2140–2195; c) M. Zhao, B. Q. Li, H. J. Peng, H. Yuan, J. Y. Wei, J. Q. Huang, *Angew. Chem. Int. Ed.* **2020**, *59*, 12636–12652; *Angew. Chem.* **2020**, *132*, 12736–12753; d) P. Geng, L. Wang, M. Du, Y. Bai, W. Li, Y. Liu, S. Chen, P. Braunstein, Q. Xu, H. Pang, *Adv. Mater.* **2022**, *34*, e2107836.
- [4] a) W. L. Bowden, L. H. Barnett, D. L. DeMuth, *J. Electrochem. Soc.* **1988**, *135*, 1; b) Z. W. Seh, J. H. Yu, W. Li, P. C. Hsu, H. Wang, Y. Sun, H. Yao, Q. Zhang, Y. Cui, *Nat. Commun.* **2014**, *5*, 5017; c) T. Takeuchi, H. Kageyama, K. Nakanishi, M. Ogawa, T. Ohta, A. Sakuda, H. Sakaebe, H. Kobayashi, Z. Ogumi, *J. Electrochem. Soc.* **2015**, *162*, A1745–A1750; d) A. Sakuda, K.

- Ohara, K. Fukuda, K. Nakanishi, T. Kawaguchi, H. Arai, Y. Uchimoto, T. Ohta, E. Matsubara, Z. Ogumi, T. Okumura, H. Kobayashi, H. Kageyama, M. Shikano, H. Sakaebi, T. Takeuchi, *J. Am. Chem. Soc.* **2017**, *139*, 8796–8799; e) B. Yan, X. Li, W. Xiao, J. Hu, L. Zhang, X. Yang, *J. Mater. Chem. A* **2020**, *8*, 17848–17882.
- [5] a) C. S. Rout, B. H. Kim, X. Xu, J. Yang, H. Y. Jeong, D. Odkhua, N. Park, J. Cho, H. S. Shin, *J. Am. Chem. Soc.* **2013**, *135*, 8720–8725; b) S. Britto, M. Leskes, X. Hua, C. A. Hebert, H. S. Shin, S. Clarke, O. Borkiewicz, K. W. Chapman, R. Seshadri, J. Cho, C. P. Grey, *J. Am. Chem. Soc.* **2015**, *137*, 8499–8508; c) L. Wu, Y. Zhang, B. Li, P. Wang, L. Fan, N. Zhang, K. Sun, *Front. Energy Res.* **2018**, *13*, 597–602; d) Z. Li, S. Ding, J. Yin, M. Zhang, C. Sun, A. Meng, *J. Power Sources* **2020**, *451*; e) Y.-Y. Liu, L. Xu, X.-T. Guo, T.-T. Lv, H. Pang, *J. Mater. Chem. A* **2020**, *8*, 20781–20802.
- [6] a) S. Wang, H. Chen, J. Liao, Q. Sun, F. Zhao, J. Luo, X. Lin, X. Niu, M. Wu, R. Li, X. Sun, *ACS Energy Lett.* **2019**, *4*, 755–762; b) L. Luo, J. Li, H. Yaghoobnejad Asl, A. Manthiram, *ACS Energy Lett.* **2020**, *5*, 1177–1185.
- [7] a) K. Koganei, A. Sakuda, T. Takeuchi, H. Sakaebi, H. Kobayashi, H. Kageyama, T. Kawaguchi, H. Kiuchi, K. Nakanishi, M. Yoshimura, T. Ohta, T. Fukunaga, E. Matsubara, *Solid State Ionics* **2018**, *323*, 32–36; b) K. Koganei, A. Sakuda, T. Takeuchi, H. Kiuchi, H. Sakaebi, *Electrochemistry* **2021**, *89*, 239–243; c) Y. Maeyoshi, K. Yoshii, M. Shikano, H. Sakaebi, *ACS Appl. Energ. Mater.* **2021**, *4*, 13627–13636; d) Y. Umemura, T. Takeuchi, H. Sakaebi, H. Kiuchi, T. Yaji, M. Katayama, *Electrochemistry* **2021**, *89*, 273–278.
- [8] a) N.-S. Choi, K. H. Yew, K. Y. Lee, M. Sung, H. Kim, S.-S. Kim, *J. Power Sources* **2006**, *161*, 1254–1259; b) X.-Q. Zhang, X.-B. Cheng, X. Chen, C. Yan, Q. Zhang, *Adv. Funct. Mater.* **2017**, *27*; c) K. Yoshii, H. Sakaebi, *Electrochemistry* **2020**, *88*, 463–467; d) A. Yano, K. Yoshii, T. Takeuchi, H. Sakaebi, *Electrochemistry* **2021**, *89*, 167–175.
- [9] a) E. Markevich, G. Salitra, A. Rosenman, Y. Talyosef, F. Chesneau, D. Aurbach, *Electrochem. Commun.* **2015**, *60*, 42–46; b) X. Li, M. Banis, A. Lushington, X. Yang, Q. Sun, Y. Zhao, C. Liu, Q. Li, B. Wang, W. Xiao, C. Wang, M. Li, J. Liang, R. Li, Y. Hu, L. Goncharova, H. Zhang, T. K. Sham, X. Sun, *Nat. Commun.* **2018**, *9*, 4509; c) Z. Zhu, Y. Tang, Z. Lv, J. Wei, Y. Zhang, R. Wang, W. Zhang, H. Xia, M. Ge, X. Chen, *Angew. Chem. Int. Ed.* **2018**, *57*, 3656–3660; *Angew. Chem.* **2018**, *130*, 3718–3722.
- [10] H. Mokudai, T. Takeuchi, H. Sakaebi, H. Kobayashi, E. Matsubara, *Sustain. Energy Fuels* **2021**, *5*, 1714–1726.
- [11] S. Hagiwara, J. Haruyama, M. Ohtani, Y. Umemura, T. Takeuchi, H. Sakaebi, *under review*.
- [12] a) C. L. Campion, W. Li, B. L. Lucht, *J. Electrochem. Soc.* **2005**, *152*; b) K. Yoshii, H. Kiuchi, N. Taguchi, M. Shikano, E. Matsubara, H. Sakaebi, *ChemElectroChem* **2020**, *7*, 4336–4342.
- [13] a) M.-H. Ryoo, G.-B. Han, Y. M. Lee, J.-N. Lee, D. J. Lee, Y. O. Yoon, J.-K. Park, *Electrochim. Acta* **2010**, *55*, 2073–2077; b) E. Markevich, G. Salitra, D. Aurbach, *ACS Energy Lett.* **2017**, *2*, 1337–1345.
- [14] K. Yoshii, N. Taguchi, T. Miyazaki, M. Shikano, H. Sakaebi, *Chem. Commun.* **2020**, *56*, 4878–4881.
- [15] M. D. Duca, C. L. Plosceanu, T. Pop, *J. Appl. Polym. Sci.* **1998**, *67*, 2125–2129.
- [16] F. Wang, J. Graetz, M. S. Moreno, C. Ma, L. Wu, V. Volkov, Y. Zhu, *ACS Nano* **2011**, *5*, 1190–1197.
- [17] E. Yamauchi, T. Takeuchi, H. Sakaebi, *Front. Energy Res.* **2019**, *7*, 38.

Manuscript received: January 6, 2022

Revised manuscript received: February 21, 2022

Accepted manuscript online: February 22, 2022